POLITECNICO DI TORINO
Repository ISTITUZIONALE

Measurements of Quench Propagation Velocity in HTS Cable for Fusion Applications Using Optical Fiber Sensors

Original
Measurements of Quench Propagation Velocity in HTS Cable for Fusion Applications Using Optical Fiber Sensors / De Stasio, M., Colombo, G., Masi, A., Breschi, M., Caponero, M.A., Celentano, G., Marchetti, M., Muzzi, L., Polimadei, A., Trotta, A., Zanon, F., De Marzi, G., Savoldi, L.. - In: IEEE TRANSACTIONS ON APPLIED SUPERCONDUCTIVITY. - ISSN 1558-2515. - 36:5(2026), pp. 1-5. [10.1109/TASC.2026.3664056]

Availability:
This version is available at: 11583/3008073 since: 2026-03-02T11:22:37Z

Publisher:
Institute of Electrical and Electronics Engineers Inc.

Published
DOI:10.1109/TASC.2026.3664056

Terms of use:

This article is made available under terms and conditions as specified in the corresponding bibliographic description in the repository

Publisher copyright

(Article begins on next page)

17 August 2026

Measurements of Quench Propagation Velocity in HTS Cable for Fusion Applications Using Optical Fiber Sensors

M. De Stasio, G. Colombo, A. Masi, M. Breschi, *Senior Member, IEEE*, M. A. Caponero, G. Celentano, M. Marchetti, L. Muzzi, *Senior Member, IEEE*, A. Polimadei, A. Trotta, F. Zanon, G. De Marzi, and L. Savoldi, *Senior Member, IEEE*

***Abstract*—Low quench propagation velocity (QPV) in high-temperature superconductors (HTS) undermines conventional voltage-based quench detection, since damaging temperatures can develop locally before appreciable voltages appear. This work investigates an ENEA aluminum slotted-core cable featuring a BRAided STack (BRAST) of REBCO tapes, instrumented with capillary-mounted fiber Bragg gratings (FBGs) in direct thermal contact with the stack, alongside conventional voltage taps. Quench experiments were carried out in liquid nitrogen flow at 77 K, with the current held constant at about 500 A. Electrical and optical signals were processed with a standardized pipeline for the onset quench: statistical thresholds for electric field, and temperature-based arrivals at FBGs. From arrival times at known positions, QPV is estimated via two independent methods based on resistive front and thermal front, respectively. Both methods yield consistent values in the range of 20–60 mm/s. Downstream, where the front is fully developed, the two estimates converge within uncertainty. These results demonstrate that embedded optical fibers provide local temperature tracking, electromagnetically immune, and minimally invasive complement to voltage taps for quench detection and QPV estimation in HTS cables for fusion-magnet applications.**

***Index Terms*—Fusion magnet, HTS magnets, quench protection, quench propagation, temperature measurement.**

Received 13 October 2025; revised 29 January 2026; accepted 9 February 2026. Date of publication 12 February 2026; date of current version 20 February 2026. This work was supported by ENI SpA through the ENI-ENEA Joint Cooperation under Agreement 5210001622, Project 5: “Quench”. *(Corresponding author: M. De Stasio.)*

M. De Stasio is with the MAHTEP Group, Department of Energy “Galileo Ferraris”, Polytechnic of Turin, 10129 Turin, Italy, and also with the Istituto Nazionale di Fisica Nucleare, sez. di Torino, 10125 Torino, Italy (e-mail: mattia.destasio@polito.it).

G. Colombo and M. Breschi are with the Department of Electrical, Electronic and Information Engineering “Guglielmo Marconi” – DEI, University of Bologna, 40126 Bologna, Italy (e-mail: gabriele.colombo6@unibo.it; marco.breschi@unibo.it).

A. Masi, M. A. Caponero, G. Celentano, M. Marchetti, L. Muzzi, A. Polimadei, and G. De Marzi are with the NUC Department, ENEA, 00044 Frascati, Italy (e-mail: andrea.masi@enea.it; michele.caponero@enea.it; giuseppe.celentano@enea.it; marcello.marchetti@enea.it; luigi.muzzi@enea.it; andrea.polimadei@enea.it; gianluca.demarzi@enea.it).

A. Trotta and F. Zanon are with Eni S.p.A, 00144 Rome, Italy (e-mail: antonio.trotta@eni.it; fabio.zanon@eni.it).

L. Savoldi is with the MAHTEP Group, Department of Energy “Galileo Ferraris”, Polytechnic of Turin, 10129 Turin, Italy, and also with Istituto Nazionale di Fisica Nucleare, sez. di Genova, 16146 Genova, Italy (e-mail: laura.savoldi@polito.it).

Color versions of one or more figures in this article are available at https://doi.org/10.1109/TASC.2026.3664056.

Digital Object Identifier 10.1109/TASC.2026.3664056

I. Introduction

HIGH-TEMPERATURE superconducting (HTS) REBCO tapes are enabling compact, high-field magnets for fusion and other applications. Recent demonstrations and roadmaps underscore the rapidly maturing HTS magnet technology for fusion applications [1], [2], [3].

In HTS conductors, the quench propagation velocity (QPV) is typically 2–3 orders of magnitude lower than in low temperature superconductors (LTS) [4], making magnet protection a challenging task. Resistive voltages develop slowly and may remain below detection thresholds while local temperatures rise to damaging levels [5], [6]. This problem complicates the use of conventional voltage-tap schemes, especially in multi-tape, multi-layer windings [7]. Quantitative studies on REBCO tapes and cables confirm low QPV both at 77 K and at low-temperature, high-field conditions, with values sensitive to architecture, stabilization, and interfacial resistance [8], [9]. Analytical and semi-empirical formulations for normal zone propagation velocity NZPV in REBCO further clarify material and operating-point dependencies relevant to magnet design [10]. Against this backdrop, alternative or complementary diagnostics to voltage taps are increasingly explored: current-distribution monitoring in CORC cables [11]; point or quasi-continuous fiber-optic sensing [12], [13]; Distributed Fiber-Optic Sensing (DFOS) [14] through both the use Rayleigh-backscattering Interrogated Optical Fiber (RIOS) [15], and other interrogation techniques focusing on enhancing sensitivity at low temperatures [16].

Fiber-Optic Sensors (FOS and DFOS) offer electromagnetic immunity, minimal invasive method and tight spatial footprints, and have been demonstrated for cryogenic strain/temperature monitoring and quench detection in superconducting cable magnets [17], [18]. Their cryogenic behavior and sensitivity have been characterized from 300 K down to a few kelvins, including metal-coated and packaged designs that enhance thermo-mechanical coupling, key for fast detection [19], [20].

Within this context, this work investigates quench detection and quench propagation velocity in an ENEA aluminum slotted-core cable with a BRAided STack (BRAST) of REBCO tapes [21], [22] using voltage taps and capillary-mounted Fiber Bragg Gratings (FBGs), cross-validating electrical and thermal fronts. The results add to the growing experimental literature on QPV in

© 2026 The Authors. This work is licensed under a Creative Commons Attribution 4.0 License. For more information, see https://creativecommons.org/licenses/by/4.0/

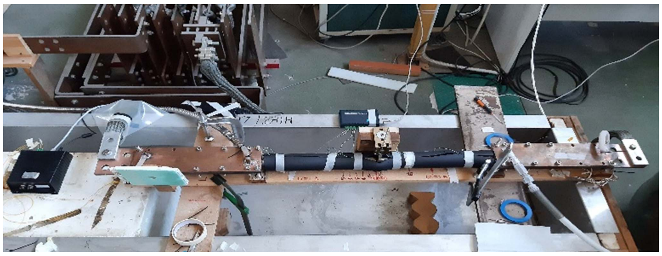

Fig. 2. The sample cable with the quench experiments equipment.

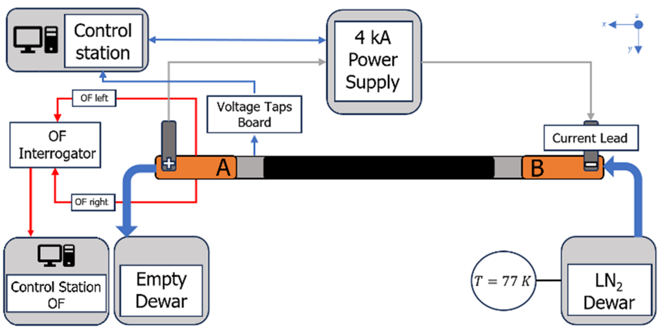

Fig. 1. Schematic of the quench test loop.

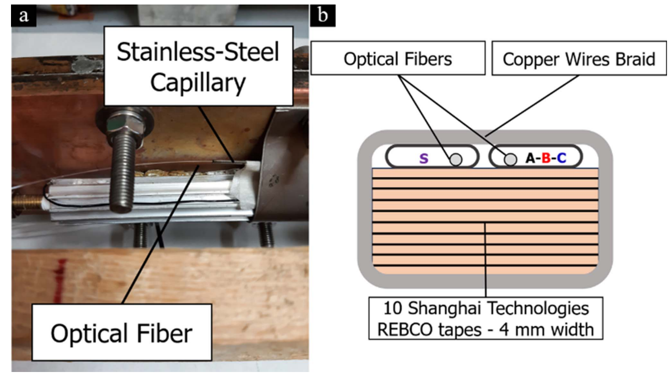

Fig. 3. Detail view of the optical fiber inside the stainless-steel capillaries (a) and the section sketch of the BRAST structure (b).

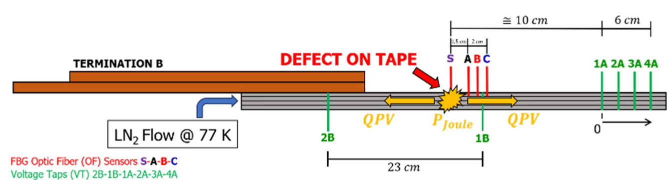

Fig. 4. Position of the OFs sensors and VTs along the cable.

REBCO conductors and cables and inform protection strategies for next-generation HTS fusion magnets.

II. Experimental Setup

This section describes the quench experimental setup, shown in Fig. 2, used to measure the QPV. The sample was positioned in the ENEA 20 kA facility and tested in liquid nitrogen flow at the operational temperature of 77 K. Fig. 1depicts the equipment and the schematic of the systems. The cable had two different terminations named A (left) and B (right).

A dewar filled with liquid nitrogen (77 K) was connected to the termination B copper plate via a flexible stainless-steel pipeline. Following the flow path within the hollow copper plate, the coolant cooled the cable via its central channel from termination B to termination A. At the end of the flow path, the liquid nitrogen was collected in an empty dewar. To reduce the thermal dispersion with the ambience along the cable, an insulating hollow sleeve was applied on the cable.

The current leads were bolted to the copper terminations and connected via large copper braids to the first 4 kA module of the power supply, monitored by the control station.

The PC control station was capable of acquiring current and voltage data with a Keithley 2000 multichannel multimeter with a shunt resistor and SCXI-1120 analog-to-digital module. The optical fibers (OFs) were interrogated with an 8 channel SENTEA DM-8125 interrogator connected to a different PC. The voltage data acquisition system and the optical interrogator were not synchronized, as they were controlled by distinct PCs. However, since the QPV is calculated using relative time intervals (time of flight) recorded within each individual system, the absolute temporal offset is irrelevant for the velocity estimation.

A. Optical Fiber and Voltage Tap Instrumentation

The two optical fibers (OF) were accurately pre-installed in their corresponding stainless-steel capillaries directly in contact with the REBCO stack (Fig. 3(b)): the left optical fiber contained a 10 mm long FBG sensor named S, whereas the right optical fiber contained an array with three different 3 mm FBGs spaced 1 cm apart, and labeled A, B and C.

Previous quench experiments [13] have confirmed the presence of a physical defect on one or more tapes at approximately 10 cm from the center of the cable, towards termination B. The pre-identified defect was exploited as the source of quench initiation.

The S-FBG was placed at the defect location, to monitor the local temperature, while the OF array in the other capillary was set 1.5 cm from the S-FBG, to track the thermal front quench propagation (Fig. 4). Because the two optical fibers used FBGs with assorted designs (i.e., with different acrylate coating thicknesses), their temperature responses differed. The calibration curve, measured in situ with respect to a calibrated thermometer, allowed to set the 77 K sensitivity to 12 pm·K^{-1} for the S-FBG and 4.8 pm·K^{-1} for the array.

The voltage taps (VTs) were directly soldered to the bottom of the HTS stack during the cable manufacturing, as thoroughly described in [13]. In these quench experiments, the most relevant VTs were the 2B-1B, the portion of cable containing the defect, and the VTs placed near the center of the cable (1A-2A, 2A-3A, 3A-4A, each $\sim$2 cm) which were used to track the resistive front quench propagation (Fig. 4).

III. Methodology

The estimation of QPV was carried out through standardized steps in which raw signals were filtered, and quench onsets and arrivals were identified on predefined criteria. To cross-validate the QPV, two independent procedures were applied: one based on voltage taps electric fields and one based on FBGs temperatures. The resulting velocities were compared to assess consistency and uncertainty.

A. QPV From Voltage Tap Electric Field

For each voltage taps segment i of length L_i, the longitudinal electric field is computed as:

$$E_i\ (t) = \frac{V_i\,(t)}{L_i} \tag{1}$$

A statistical threshold is derived from a pre quench window W at the beginning of the run, where the electric field is approximately constant, lasting about 60–70 s. Let N_i denote the number of the time samples in W, with a sampling interval of 100 ms. The mean and the standard deviation are:

$$\bar{E}_i = \frac{1}{N_i} \cdot \sum\nolimits_{k\in W} E_i\,(t_k) \tag{2}$$

$$\sigma_{\bar{E}_i} = \sqrt{\frac{1}{N_i - 1} \cdot \sum\nolimits_{k\in W} \left[E_i\,(t_k) - \bar{E}_i\right]^2} \tag{3}$$

The electric field threshold is then:

$$E_{thr,i} = \bar{E}_i\ + N_E \cdot \sigma_{\bar{E}_i} \tag{4}$$

with $N_E =\ 3$ the multiplier for the standard deviation, the criterion provides high confidence (low false positive probability) onset detection.

To suppress spurious triggers, the electric field time derivative is also considered. Using the central difference scheme with the sampling period Δt_N:

$$\dot{E}_i\,(t_k) = \frac{E_i\,(t_{k+1}) - E_i\,(t_{k-1})}{2\Delta t_N} \approx \frac{dE_i\,(t)}{dt} \tag{5}$$

From the same pre-quench window W, the mean and the standard derivation are computed using the electric field time derivative and substituting it in (2), (3) and (4) and obtaining the same $\dot{E}_{thr}$ form of (4), with $N_{\dot{E}} = 5$, a conservative choice to minimize false alarms.

Global thresholds $E_{thr}, \dot{E}_{thr}$ are taken as the mean across segments. To be sure to measure the well-developed front of the quench, a factor of 4 of the E_{thr} is set, with the final threshold value of approximately 40 μV/cm. Next, the arrival time $t_{quench,i}$ at which the segment i satisfies the threshold criteria are recorded. The quench propagation velocity for the segment i is then estimated from the time of flight between the signal onsets of two consecutive, adjacent sensors:

$$QP\,V_i = \frac{L_i}{\Delta t_{quench,i}} \tag{6}$$

B. QPV From FBGs Temperature Transient

The temperature threshold is set at 93 K, corresponding to the nominal zero field superconductor-to-normal transition of these tapes [23]; above this value the conductor is considered resistive. This yields a simpler, more linear procedure: once each FBG sensor meets the prescribed temperature criterion, its arrival time $t_{quench,i}$ is recorded. The quench-propagation velocity is computed with the same (6).

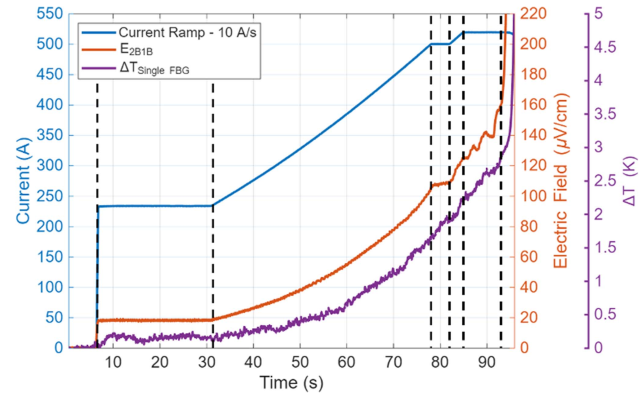

Fig. 5. Time evolution of the electric field measured by the voltage tap within the defect zone (orange) and the temperature rise detected by the single FBG sensor on the defect (violet) during Run 1.

IV. Results and Discussion

This section reports experimental observation and interpretations. Both diagnostics capture a coherent propagation of the normal zone. The QPV estimates from VT electric fields and from the FBG temperature transient agree within the stated uncertainties.

Two runs were performed with the same current ramp of about 10 A/s up to steady state of roughly 520 A, both starting after an initial step to approximately 240 A.

Fig. 5 illustrates the time evolution of the temperature rise detected by the single FBG positioned on the defect, alongside the electric field measured by the E1B2B voltage tap. Upon current injection, the onset of resistive behavior is immediately observable due to the localized reduction of the critical current at the defect site; consequently, the electric field mirrors the current ramp. As expected, the FBG located in the defect zone registers a temperature increase caused by Joule heating resulting from local current redistribution, following the same trend as the electric field.

As can be seen in Fig. 6, voltage taps and FBG sensors confirm similar trends in the other parts of the cable. The voltage taps are stable up to approximately 60 s. Subsequently, a pre-quench precursor phenomenon appears, anticipating the quench onset in probes 1A-2A (in black), while the other two probes, which react later to the trigger, show values close to noise. In the bottom panel, the thermal response of FBG A (black) shows an increase from the initial value due to its closer proximity to the defect, while FBG B and FBG C remain approximately constant until the onset of thermal runaway. The quench event, therefore, starts from the defective area and propagates towards the center. Fig. 7 zooms in on the quench onset with the selected thresholds overlaid. In the electric field panel, the signal across the defect (E_{2B1B}, in purple) grows first, while among the short spans the 1A-2A trace (black) crosses the threshold earliest, followed by 2A-3A (red) and 3A-4A (blue), as the quench propagates.

Similarly, the single FBG at the defect rises sharply, staying at 3 K during the ramp, and FBG A, the nearest of the array to

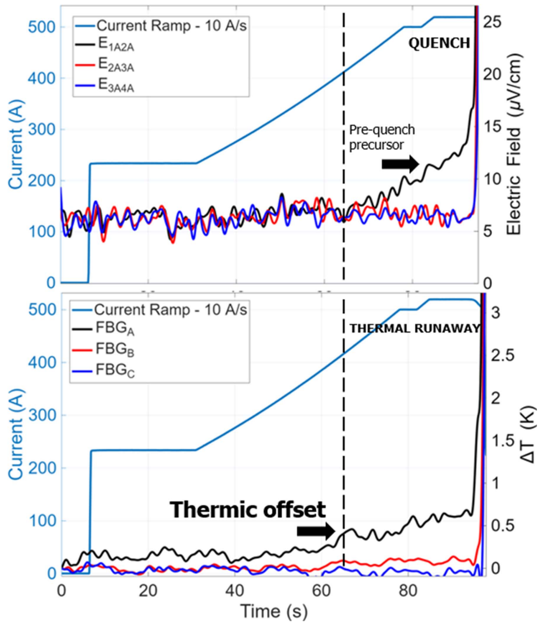

Fig. 6. Trends of the voltage taps (upper) and FBG sensors (lower) of the Run 1.

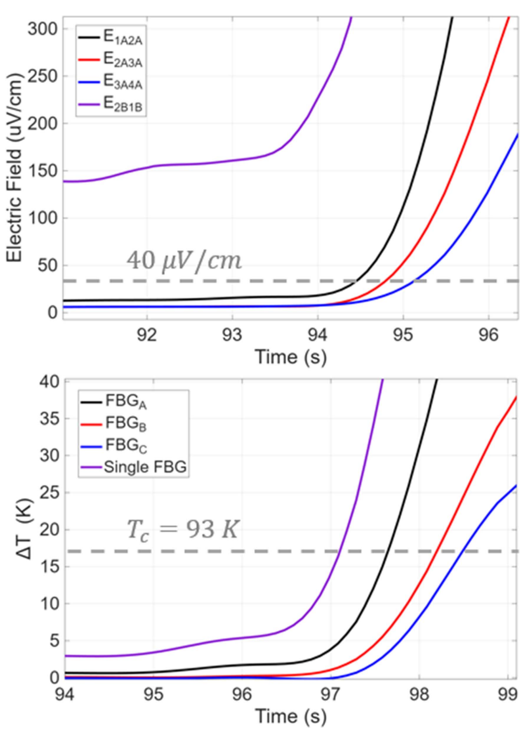

Fig. 7. Detail of the quench onset of the voltage taps (upper) and FBG sensors (lower) of the run 1.

the defect, shows the first local temperature increase; FBG B and FBG C stay near baseline until the approach of the thermal runaway.

The QPV values obtained from the two runs are summarized in Fig. 8. Green symbols refer to the voltage taps measurements, red symbols to the FBG sensor measurements. All values fall in the range of tens of mm/s (20–60 mm/s), as expected in literature [6], [24].

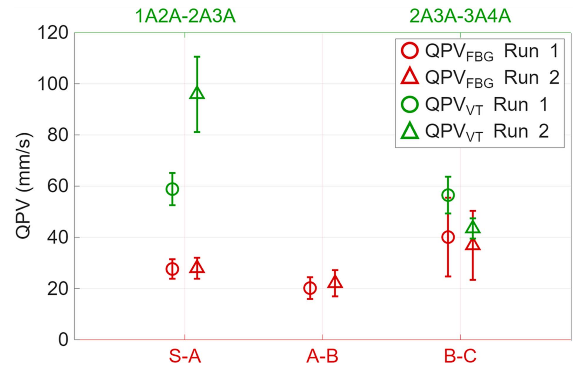

Fig. 8. Quench-propagation velocity (QPV) from electrical (green) vs thermal (red) methods.

The central region (1A2A-2A3A) shows the largest velocity, which is consistent with the development of a fast resistive front once the defect-initiated zone reaches the cable center.

Thermal estimates of S-A are lower than 1A2A-2A3A by roughly a factor of 2, reflecting the different nature of the two fronts. The two procedures deliver consistent QPV values while providing complementary information of the scenario.

However, the response times depend strongly on the chosen thresholds and are not relevant for the scope of this work. For clarity, a threshold-sensitivity study is therefore needed to quantify how, and by how much, the inferred timings change with the selection criteria. Thresholds were intentionally set to prioritize propagation tracking over onset detection. Further experiments may be devoted to understanding how physical effects such as thermal inertia, thermal capacity of the materials and local cooling contribute to adding to the delay after the quench onset between the methods. It is equally important to note that such a low voltage threshold would be impractical inside a tokamak due to significant inductive noise; in such environments, fiber-optic sensing may play a crucial role in tracking small temperature variations. However, while point sensors such as the FBGs employed here are effective for local QPV measurement, we acknowledge that practical magnet protection would require Quasi-Distributed or Distributed Fiber Optic Sensing to monitor the full conductor length.

V. Conclusion

This work presents the experimental setup, methodology and analysis used to determine QPV. An ENEA aluminum slotted core cable with a BRAST of REBCO tapes has been subjected to different quench run in LN_2 flow at 77 K and 500 A approximately. Capillary-mounted optical fiber with FBG array, integrated into the BRAST structure, were used to monitor local temperature rise of the stack and track the thermal front propagation, while the resistive front was monitored though conventional voltage taps. The QPV was computed for both runs using both procedures and the results were compared: the measured values reflect the range accepted in literature of tens of mm/s, specifically 20–60 mm/s. Where the fronts are fully established, the electrical and thermal estimates seem to converge, and may support the view that, under ideal conditions, the resistive and thermal fronts propagate essentially the same speed.

REFERENCES

[1] Z. Y. Li et al., "21.7-T large-scale high-temperature superconducting toroidal magnet for tokamak fusion application," *IEEE Trans. Appl. Supercond.*, vol. 35, no. 6, Sep. 2025, Art. no. 4203006, doi: 10.1109/TASC.2025.3573869.

[2] N. Mitchell et al., "Superconductors for fusion: A roadmap," *Supercond. Sci. Technol.*, vol. 34, no. 10, Oct. 2021, Art. no. 103001, doi: 10.1088/1361-6668/ac0992.

[3] L. Giannini et al., "Advances in magnet and shielding designs for fusion and high energy physics applications," *Fusion Eng. Des.*, vol. 214, 2025, Art. no. 114899, doi: 10.1016/j.fusengdes.2025.114899.

[4] J. van Nugteren et al., "Measurement and analysis of normal zone propagation in a ReBCO coated conductor at temperature below 50 K," *Phys. Procedia*, vol. 67, pp. 945–951, 2015, doi: 10.1016/j.phpro.2015.06.159.

[5] T. Yang and X. Wang, "Enhanced visualization of quench dynamics of HTS coils through embedded and distributed fiber optical sensing," *Measurement*, vol. 242, 2025, Art. no. 116034, doi: 10.1016/j.measurement.2024.116034.

[6] M. Marchevsky, "Quench detection and protection for high-temperature superconductor accelerator magnets," *Instruments*, vol. 5, no. 3, Aug. 2021, Art. no. 27, doi: 10.3390/instruments5030027.

[7] J. Schwartz, "Quench in high temperature superconductor magnets," in *Proc. Workshop Accel. Magnet Supercond., Des. Optim.*, Geneva, Switzerland, 2013, pp. 21–29, doi: 10.5170/CERN-2013-006.21.

[8] C. Lacroix et al., "Normal zone propagation in various REBCO tape architectures," *Supercond. Sci. Technol.*, vol. 35, no. 5, May 2022, Art. no. 055009, doi: 10.1088/1361-6668/ac56ff.

[9] A. Zappatore et al., "Modeling quench propagation in the ENEA HTS cable-in-conduit conductor," *IEEE Trans. Appl. Supercond.*, vol. 30, no. 8, Dec. 2020, Art. no. 4603307, doi: 10.1109/TASC.2020.3001035.

[10] M. Bonura and C. Senatore, "An equation for the quench propagation velocity for high field magnet use of REBCO coated conductors," *Appl. Phys. Lett.*, vol. 108, no. 24, 2016, Art. no. 242602, doi: 10.1063/1.4954165.

[11] R. Teyber et al., "Current distribution monitoring enables quench and damage detection in superconducting fusion magnets," *Sci. Rep.*, vol. 12, 2022, Art. no. 22503, doi: 10.1038/s41598-022-26592-2.

[12] E. E. Salazar et al., "Fiber optic quench detection for large-scale HTS magnets demonstrated on VIPER cable during high fidelity testing at the SULTAN facility," *Supercond. Sci. Technol.*, vol. 34, no. 3, Mar. 2021, Art. no. 035027, doi: 10.1088/1361-6668/abdba8.

[13] A. Masi et al., "Integration of optical sensors for quench detection in HTS stacks and cables for fusion applications," *IEEE Trans. Appl. Supercond.*, vol. 35, no. 5, Aug. 2025, Art. no. 4201705, doi: 10.1109/TASC.2025.3536443.

[14] G. Colombo et al., "Comparative study on distributed fiber optic–based quench detection schemes for HTS cables for fusion magnets," *IEEE Trans. Appl. Supercond.*, vol. 35, no. 5, Aug. 2025, Art. no. 4201405, doi: 10.1109/TASC.2025.3532931.

[15] F. Scurti and J. Schwartz, "Optical fiber distributed sensing for high temperature superconductor magnets," in *Proc. 25th Opt. Fiber Sensors Conf.*, 2017, pp. 1–4, doi: 10.1117/12.2265947.

[16] R. Vallifuoco et al., "High spatial resolution distributed Brillouin measurements at cryogenic temperatures," *IEEE Trans. Instrum. Meas.*, vol. 74, 2025, Art. no. 9536809, doi: 10.1109/TIM.2025.3613892.

[17] A. Chiuchiolo et al., "Fiber Bragg grating cryosensors for superconducting accelerator magnets," *IEEE Photon. J.*, vol. 6, no. 6, Dec. 2014, Art. no. 0600310, doi: 10.1109/JPHOT.2014.2343994.

[18] S. A. Adibi et al., "Multi-sensor quench detection system for an HTS slotted superconducting cable," *IEEE Trans. Appl. Supercond.*, vol. 34, no. 3, May 2024, Art. no. 9000304, doi: 10.1109/TASC.2023.3340130.

[19] R. R. Kumar et al., "Performance evaluation of metal-coated fiber Bragg gratins sensors for sensing cryogenic temperature," *Cryogenics*, vol. 48, no. 3/4, pp. 142–147, Mar. 2008, doi: 10.1016/j.cryogenics.2008.02.007.

[20] Z. S. Guo et al., "Cryogenic temperature characteristic of the fiber Bragg grating sensors," *Cryogenics*, vol. 52, no. 10, pp. 457–460, May 2012, doi: 10.1016/j.cryogenics.2012.04.012.

[21] L. Muzzi et al., "Design and feasibility assessment of an HTS sector shaped high-current conductor for fusion coils," *IEEE Trans. Appl. Supercond.*, vol. 33, no. 5, Aug. 2023, Art. no. 4200106, doi: 10.1109/TASC.2023.3236592.

[22] G. Celentano et al., "Design of an industrially feasible twisted stack HTS cable-in-conduit conductor for fusion application," *IEEE Trans. Appl. Supercond.*, vol. 24, no. 3, Jun. 2014, Art. no. 4601805, doi: 10.1109/TASC.2013.2287910.

[23] B. Taheri et al., "Sensitivity of *REBCO* tapes and thin film to γ-irradiation," *IEEE Trans. Appl. Supercond.*, vol. 34, no. 5, Aug. 2024, Art. no. 6600105, doi: 10.1109/TASC.2023.3338590.

[24] A. Zappatore et al., "DC and quench performance assessment from the EUROfusion HTS quench experiment campaign and projection to magnet operation," *Cryogenics*, vol. 150, Sep. 2025, Art. no. 104158, doi: 10.1016/j.cryogenics.2025.104158.

Open Access funding provided by 'Politecnico di Torino' within the CRUI CARE Agreement